

## Article

# Mixed Oxides NiO/ZnO/Al<sub>2</sub>O<sub>3</sub> Synthesized in a Single Step via Ultrasonic Spray Pyrolysis (USP) Method

Duygu Yeşiltepe Özcelik <sup>1</sup>, Burçak Ebin <sup>2</sup>, Srečko Stopić <sup>3,\*</sup>, Sebahattin Gürmen <sup>1</sup> and Bernd Friedrich <sup>3</sup>

<sup>1</sup> Department of Metallurgical and Materials Engineering, Faculty of Chemistry and Metallurgy, Ayazağa Campus, Istanbul Technical University, İstanbul 34469, Turkey; yesiltepe15@itu.edu.tr (D.Y.Ö.); gurmen@itu.edu.tr (S.G.)

<sup>2</sup> Nuclear Chemistry and Industrial Material Recycling, Department of Chemistry and Chemical Engineering, Chalmers University of Technology, S-412 96 Gothenburg, Sweden; burcak@chalmers.se

<sup>3</sup> Department of Process Metallurgy and Metal Recycling, RWTH Aachen University, 52056 Aachen, Germany; bfriedrich@ime-aachen.de

\* Correspondence: sstopic@ime-aachen.de; Tel.: +49-176-7826-1674

**Abstract:** Mixed oxides have received remarkable attention due to the many opportunities to adjust their interesting structural, electrical, catalytic properties, leading to a better, more useful performance compared to the basic metal oxides. In this study, mixed oxides NiO/ZnO/Al<sub>2</sub>O<sub>3</sub> were synthesized in a single step via the ultrasonic spray pyrolysis method using nitrate salts, and the temperature effects of the process were investigated (400, 600, 800 °C). The synthesized samples were characterized by means of scanning electron microscopy, energy-dispersive spectroscopy, X-ray diffraction and Raman spectroscopy analyses. The results showed Al<sub>2</sub>O<sub>3</sub>, NiO–Al<sub>2</sub>O<sub>3</sub> and ZnO–Al<sub>2</sub>O<sub>3</sub> systems with spinel phases. Furthermore, the Raman peaks supported the coexistence of oxide phases, which strongly impact the overall properties of nanocomposite.

**Keywords:** nanocomposite; ultrasonic spray pyrolysis; mixed oxides; NiAl<sub>2</sub>O<sub>4</sub>; ZnAl<sub>2</sub>O<sub>4</sub>



**Citation:** Yeşiltepe Özcelik, D.; Ebin, B.; Stopić, S.; Gürmen, S.; Friedrich, B. Mixed Oxides NiO/ZnO/Al<sub>2</sub>O<sub>3</sub> Synthesized in a Single Step via Ultrasonic Spray Pyrolysis (USP) Method. *Metals* **2022**, *12*, 73. <https://doi.org/10.3390/met12010073>

Academic Editor: Chang Woo Lee

Received: 20 November 2021

Accepted: 29 December 2021

Published: 2 January 2022

**Publisher's Note:** MDPI stays neutral with regard to jurisdictional claims in published maps and institutional affiliations.



**Copyright:** © 2022 by the authors. Licensee MDPI, Basel, Switzerland. This article is an open access article distributed under the terms and conditions of the Creative Commons Attribution (CC BY) license (<https://creativecommons.org/licenses/by/4.0/>).

## 1. Introduction

Nanocomposites are a research hotspot at present, with various applications in day-to-day technologies. A further improvement in properties is achieved when one of the components in the composite is reduced to the nanoscale (~1–100 nm). With an increased surface area, and the quantum effects that arise at this scale, this nanocomposite offers better electrical, mechanical, chemical, optical, and magnetic properties. Their melting point and dielectric constant can change when particles reach nanometre sizes [1,2]. Mixed-oxide nanocomposites are studied due to their potential for an enhanced functional performance in photocatalysis, sensors and other optoelectronic device applications [3]. The combination of two or more metals in an oxide matrix can produce materials with novel physical and chemical properties, leading to an increased performance in various technological applications [4]. Among the various mixed oxides, nickel oxide (NiO), zinc oxide (ZnO) and alumina (Al<sub>2</sub>O<sub>3</sub>) have been a focus in the semiconductor and chemical and petrochemical industry due to their distinguished electronic, magnetic and chemical properties. These mixed metal oxides are widely used in the field of adsorption and catalysis. They are used in many catalytic reactions in chemical and petrochemical industries, including cracking, hydrogenation dehydrogenation, reforming, and dehydration [5,6].

NiO is an eco-friendly, stable, low-cost and wide-bandgap material [7,8]. NiO nanoparticles have been a great candidate for ferroelectric p-type semiconductors with a wide band gap (3.6–4.0 eV). Recently, NiO materials have been used in technological fields such as electrochromic test equipment, supercapacitors, rechargeable lithium ion batteries as electrodes, magnetic recorders, photocatalysts, adsorbents, etc. [9]. ZnO nanoparticles, which have a large band gap (3.37 eV) and large exciton binding energy of 60 meV at room temperature,

have a wide range of uses [10]. ZnO is of great interest due to its potential applications in various fields, such as gas sensors, biosensors, catalysis, solar batteries and as electronic, piezoelectric and optical devices, as well as in ultraviolet (UV) protection, cosmetics and paints [9,11,12]. Al<sub>2</sub>O<sub>3</sub> has unique properties that made it one of the most important engineering materials of the late twentieth century, including chemical stability, high hardness, and a high melting temperature, which allowed it to be used in many areas, especially in the manufacture of ceramics, refinement, and optics. It is found in several patterns that differ from each other in terms of their crystalline structure and physical and chemical properties, in addition to its various applications [13]. Al<sub>2</sub>O<sub>3</sub> is one of the most common ceramic materials, used as a catalyst, adsorbent and abrasion-resistant coating [14]. It is a very important adsorbent, with surface activity species (Al<sup>3+</sup>, O<sup>2-</sup>, OH<sup>-</sup> group decomposed and proton defects), and acts as an adsorption center for different gases. In this regard, in the gas-sensing process, Al<sub>2</sub>O<sub>3</sub> increases the adsorption amount of oxygen and the tested gases. Moreover, transition metal oxides deposited on the Al<sub>2</sub>O<sub>3</sub> surface have a high dispersion form [15]. The ZnO/Al<sub>2</sub>O<sub>3</sub> nanocomposite is used for UV emission [16]. Composites from Al<sub>2</sub>O<sub>3</sub>-NiO systems with spinel-phase nickel aluminate (NiAl<sub>2</sub>O<sub>4</sub>) are used as catalysts or precatalysts for steam reformation or as electrode materials in high-temperature fuel cells due to their unusual conductivity [17]. Zinc aluminate (ZnAl<sub>2</sub>O<sub>4</sub>), is a mixed oxide with spinel structure that is currently used as high-temperature material, sensors, electronic and optical materials, and catalyst support [18]. ZnAl<sub>2</sub>O<sub>4</sub> has a much higher photocatalytic activity than a single oxide [19]. NiO/ZnO/Al<sub>2</sub>O<sub>3</sub> nanocomposites are used as catalysts in industrial processes such as hydrogenation and dehydrogenation reactions, petroleum refining, deoxygenation, CO<sub>2</sub> reduction and fuel cells [20,21]. Other applications, such as protective barriers, electrochromic material and sensors, are also available [22].

Two strategies are used in the synthesis of nanomaterials: top-down and bottom-up. In the top-down approach, bulk particulate materials are broken down into smaller and smaller particles. This approach is mostly applicable for solids and dispersed solids. In the bottom-up approach, nanoparticles are built up one atom or molecule at a time. This is applied mostly in the gas or liquid phases. Usually, the nanoparticles obtained by the bottom-up approach are purer and have a better control of particle size and surface chemistry [23]. Different methods, such as sol-gel, hydrothermal, homogeneous precipitation [3], solid-state reaction, sonochemical method and the ultrasonic spray pyrolysis (USP) method, are used to produce nanocomposites [2,14]. The method selection depends on the ease of the method, the type and properties of the nanocomposite, etc., in its preparation. The growth of controlled-size nanoparticles is an intricate task. The reported methods have many drawbacks, since they need complex equipment, higher processing temperature and a longer reaction time [12]. The spray pyrolysis method consists of sequential and continuous processes of nebulization, precipitation, pyrolysis, and sintering to construct particles with homogeneous compositions, allowing for the precise control of solid-state reaction output and chemical composition [24,25]. Compared with the traditional nozzle, an ultrasonicator can nebulize the coating solution into ultra-tiny and foggy droplets between 1 µm and 5 µm with more homogeneous nano- and submicron particle sizes [25]. The USP technique is used for its low cost and its simplicity to implement, to fabricate oxide with good qualities [26].

Lu et al. [27] synthesized a flower-like NiO/ZnO composite by a two-step hydrothermal process, where the NiO nanosheets grew on the surface of the ZnO hexagonal nanorods. Kaur et al. [28] developed a gas sensor based on branch-like NiO/ZnO heterostructures. The synthesis process contained the growth of NiO nanowires on a substrate via the vapour-liquid-solid mechanism, and then the formation of ZnO nanowires directly on the former NiO nanowires using the vapour-solid technique. Zhu et al. [29] synthesized a hierarchical flower-like NiO/ZnO composite via a one-step hydrothermal approach. The gas-sensing properties of the NiO/ZnO composite were investigated via exposure to different ethanol concentrations at various operating temperatures. Li et al. [30] synthesized nanostructured ZnO/NiO microspheres with a nanorods-composed shell and a microsphere yolk via the

controlled calcination treatment of bimetallic organic frameworks in air. Kim et al. [31] prepared a three-dimensional (3D) sphere-like structured ZnO–NiO nanocomposites via a simple, one-pot solution process. They investigated the effects of annealing temperatures on the morphological properties of sphere-like structured ZnO–NiO nanocomposites. Mahajan et al. [32] produced NiO/ZnO composite powder using a solid-state reaction method. The dielectric constant of the composite powder was measured using impedance spectroscopy. From room-temperature dielectric measurements, it was observed that, at 1 kHz frequency, the dielectric constant for ZnO, NiO and NiO/ZnO composite powder was 8.3, 43.9, and 14.9, respectively. Li et al. [15] combined NiO and Al<sub>2</sub>O<sub>3</sub> into one system and investigated the gas-sensing properties of the composite. The activity species on its surface are centers of adsorption for different gases. Lei et al. [33] present a facile and low-cost method to synthesize hierarchical porous ZnO–Al<sub>2</sub>O<sub>3</sub> microspheres through a hydrothermal route. The hierarchical porous ZnO–Al<sub>2</sub>O<sub>3</sub> composite has a higher adsorption ability compared with pure ZnO and Al<sub>2</sub>O<sub>3</sub>. Ullah et al. [34] produced ZnO–Al<sub>2</sub>O<sub>3</sub> composite oxides with an improved structure, synthesized by the freeze-drying modified cation–anion couple hydrolysis (CADH) technique and supported by Ni, and it was determined that the desulfurization capacity is high. Li et al. [35] compared NiO/ $\gamma$ -Al<sub>2</sub>O<sub>3</sub> nanofibers with TiO<sub>2</sub> nanoparticles, one of the most commonly used photocatalysts. Considering their recyclability and structural integrity, it is understood that NiO/ $\gamma$ -Al<sub>2</sub>O<sub>3</sub> may have practical photocatalyst applications in environmental controls such as air/water pollution.

In this study, mixed oxides NiO/ZnO/Al<sub>2</sub>O<sub>3</sub> were synthesized via the USP method and a series of tests were conducted to characterize the nanocomposite particles. To the best of our knowledge, it is still a great challenge to utilize a simple and facile route to synthesize the mixed oxide nanocomposite. This study aims to introduce a single-step, facile process route for the production of new, mixed-oxide nanocomposite particles.

## 2. Materials and Methods

Mixed oxides NiO/ZnO/Al<sub>2</sub>O<sub>3</sub> were synthesized via the USP method using an aqueous solution of nitrate salts under a 1 L min<sup>−1</sup> air flow rate at different temperatures (400, 600, 800 °C). The chemicals used in the preparation of the mixed oxides were high-purity from Sigma Aldrich. The salts used were nickel nitrate hexahydrate (Ni(NO<sub>3</sub>)<sub>2</sub>·6H<sub>2</sub>O), zinc nitrate hexahydrate (Zn(NO<sub>3</sub>)<sub>2</sub>·6H<sub>2</sub>O), and aluminium nitrate nonahydrate (Al(NO<sub>3</sub>)<sub>3</sub>·9H<sub>2</sub>O). The nitrate salts were dissolved in distilled water with a concentration of 0.2 M. Then, the solution was magnetically stirred at room temperature for 15 min at 500 rpm. Experimental parameters of syntheses are summarized in Table 1.

**Table 1.** Experimental parameters.

Process Temperature (°C)	Ni(NO <sub>3</sub> ) <sub>2</sub> ·6H <sub>2</sub> O (M)	Zn(NO <sub>3</sub> ) <sub>2</sub> ·6H <sub>2</sub> O (M)	Al(NO <sub>3</sub> ) <sub>3</sub> ·9H <sub>2</sub> O (M)	Ultrasonic Frequency (MHz)	Air Flow Rate (L min <sup>−1</sup> )
400	0.2	0.2	0.2	1.3	1
600	0.2	0.2	0.2	1.3	1
800	0.2	0.2	0.2	1.3	1

The experimental setup is illustrated in Figure 1. The set up consists of an ultrasonic atomizer, quartz tube, furnace, and collection chamber. The quartz tube was placed inside the furnace (Nabertherm, R50/500/12–B) with a temperature control of  $\pm 1$  °C. An ultrasonic nebulizer with a frequency of 1.3 MHz (Ramine Baghai Instrumentation, Pyrosol 7901, Meylan, France) was used for aerosol generation from the precursor solution. The aerosols were carried into the preheated furnace by air. The removal of water occurred in the first sections of the furnace. Continuous thermal decomposition reaction of nitrates to oxides took place in the quartz tube at 400, 600 and 800 °C. The particles were collected in collection chambers in distilled water.

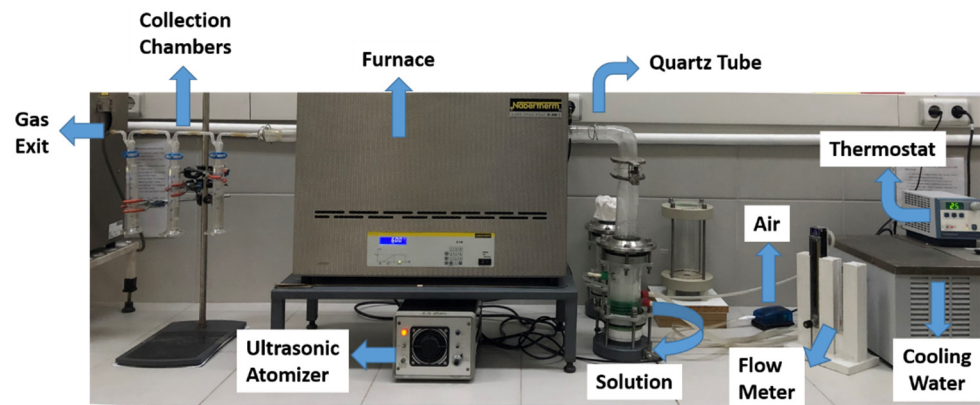


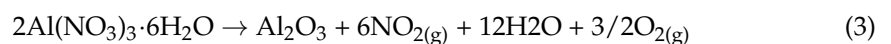
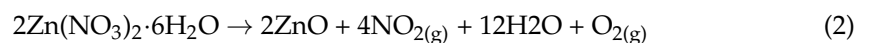
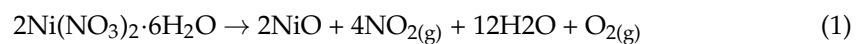
Figure 1. General view of the experimental setup.

The thermodynamics of the decomposition reaction of metal nitrates were investigated by HSC Chemistry software (HSC Chemistry 10, Metso Outotec, Helsinki, Finland). The crystal structures of the synthesized NiO/ZnO/Al<sub>2</sub>O<sub>3</sub> were analysed with an X-ray diffractometer (XRD: Rigaku MiniFlex, Tokyo, Japan), using Cu K<sub>α</sub> radiation ( $\lambda = 1.5405 \text{ \AA}$ ). The samples were scanned in the  $2\theta$  range of 5–90°. The step angle and scan speed were kept at 0.02° and 2° min<sup>-1</sup>. Morphology investigations of the specimens were inspected with scanning electron microscopy (SEM: FESEM; JSM 7000F, JEOL Ltd., Tokyo, Japan). The working distance of the samples from the tip of the electron gun and the accelerating voltage was adjusted to 10–15 mm and 5 kV, respectively. Energy dispersive X-ray spectroscopy (EDS: Oxford INCA, Abingdon, UK) was also used to investigate the chemical composition of mixed oxides. Raman spectrums of mixed oxides NiO/ZnO/Al<sub>2</sub>O<sub>3</sub> composite specimens were measured using Raman spectrometer (Horiba HR800UV, Kyoto, Japan) equipped with a 632 nm laser for sample excitation.

### 3. Results and Discussion

#### 3.1. Thermodynamic Analysis

The possible reaction equations during the decomposition of metal nitrates to mixed metal oxide particles were assumed as shown in Equations (1)–(3). The Gibb's free energy ( $\Delta G^\circ$ ), the reaction equilibrium constant and reaction equilibrium amounts were computed by HSC Chemistry software for the temperature range of 0–1000 °C. In spray pyrolysis, aerosol droplets of the dissolved salts are carried into the furnace. When the droplets meet the hot zone, the salt precipitates due to the evaporation of solvent, which is water, and then pyrolysis reactions take place. Thus, the reaction thermodynamic was calculated using metal salts. Figure 2 shows the changes in the Gibbs free energies and the logarithmic values of reaction equilibrium constant ( $K_p$ ; partial pressure of reaction products divided by partial pressure of reactants in equilibrium condition) as a function of temperature.



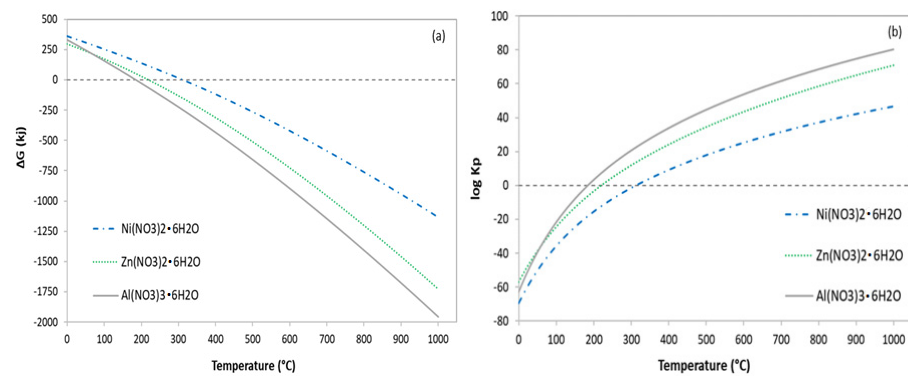


**Figure 2.** Thermodynamic investigation of the decomposition reactions for Ni, Zn and Al-nitrate salts to oxide forms; changes of (a) Gibbs free energy and (b) reaction equilibrium constant as a function of temperature.

At the chosen reaction temperatures, the Gibbs free energies for the decomposition of Al-, Zn- and Ni-nitrate salts to their oxides obtain negative values at temperatures above 185, 220 and 314 °C, respectively. Considering the continuous gas flow and their effect on removing the gas reaction products around the nucleated particles, the obtained reactions are spontaneous at the chosen process temperatures.

The changes in reaction equilibrium amounts caused by an elevation of temperature are given in Figure 3. According to the thermodynamic results, the formation of  $\text{Al}_2\text{O}_3$  starts at a lower temperature than the others, and ZnO nucleation follows. In a tube furnace, as used in the experiments, there is a slight temperature gradient from the entry into the inner zone. Thus,  $\text{Al}_2\text{O}_3$  should primarily nucleate, and the following decompositions of metal salts can lead to the formation of metal (zinc and nickel) aluminates.

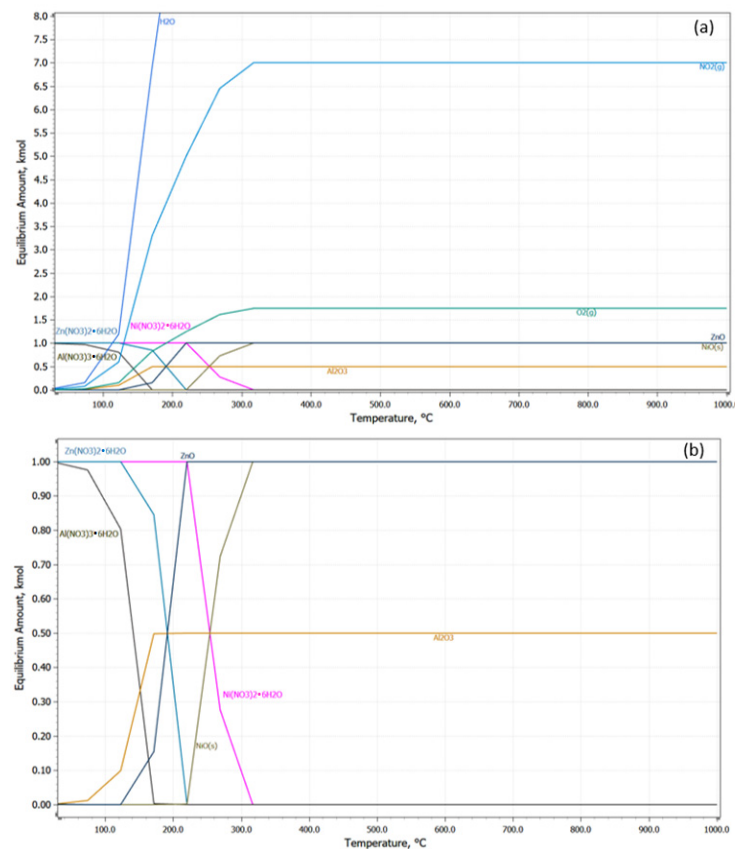


**Figure 3.** (a) Calculated reaction equilibrium amounts for decomposition reactions of metal nitrates. (b) Shows the magnified region of the graphic (a) (between Equilibrium amounts, kmol 0.00–1.00).

### 3.2. XRD Analysis

The XRD patterns of samples via produced at different temperatures are shown in Figure 4. X'Pert Highscore Plus was used to assign the phases. The diffraction peaks of mixed oxides were identified and assigned to crystalline alumina ( $\text{Al}_2\text{O}_3$ ), a cubic  $\text{NiAl}_2\text{O}_4$  (space group:  $\text{Fd-3m}$ ) and a cubic  $\text{ZnAl}_2\text{O}_4$  (space group:  $\text{Fd-3m}$ ).

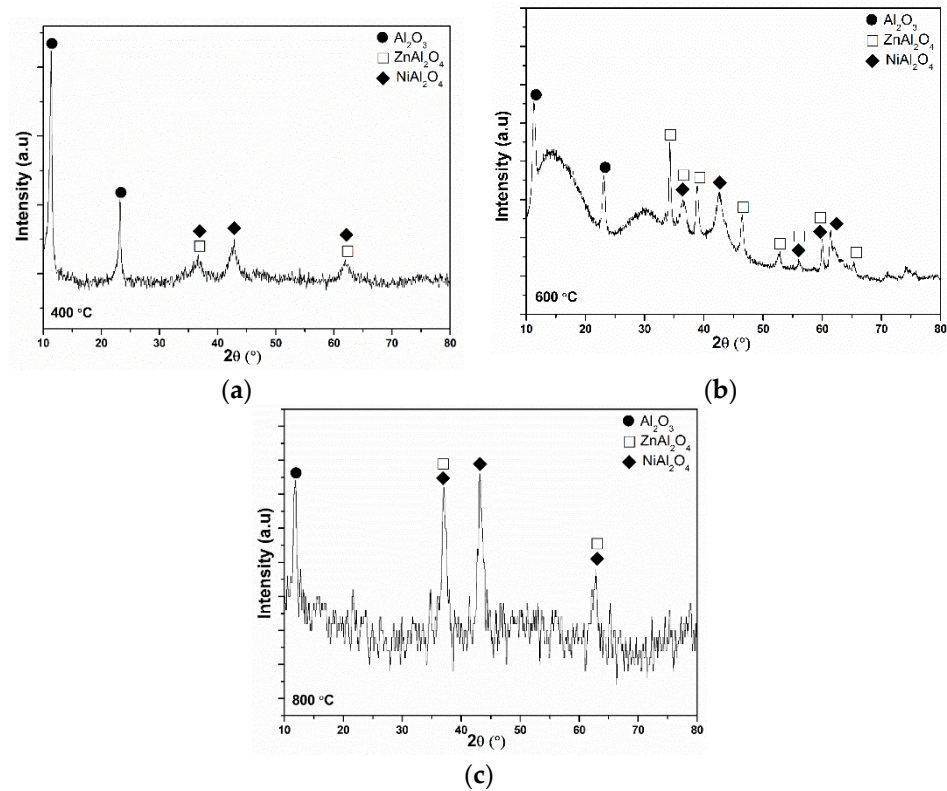


**Figure 4.** XRD patterns of mixed oxides  $\text{NiO}/\text{ZnO}/\text{Al}_2\text{O}_3$  obtained with different reaction temperature: (a) 400 °C; (b) 600 °C; (c) 800 °C.

$\text{Al}_2\text{O}_3$  peaks' positions were identified by comparing with JCPDS file No. 00-046-1215. The peaks of the  $\text{Al}_2\text{O}_3$  were the hkl reflection of 010 and 021 at  $2\theta$  of  $11.09^\circ$  and  $23.68^\circ$ , respectively.  $\text{ZnAl}_2\text{O}_4$  peaks' positions were identified by comparison with JCPDS file No. 00-005-0669. The characteristic peaks at  $2\theta$  of  $31.2^\circ$ ,  $36.75^\circ$ ,  $44.7^\circ$ ,  $49.1^\circ$ ,  $55.6^\circ$ ,  $59.3^\circ$ , and  $65.3^\circ$  are corresponding to (220), (311), (400), (331), (422), (511), and (440) diffraction planes [18,36,37]. The peaks of the  $\text{ZnAl}_2\text{O}_4$  were the hkl reflection of 311 and 440.  $\text{NiAl}_2\text{O}_4$  peaks' positions were identified by comparison with the diffraction data from the JCPDS file No. 10-0339. The major peaks for a cubic phase  $\text{NiAl}_2\text{O}_4$  (space group  $\text{Fd-3m}$ ) were the hkl reflections of 311, 400, 422 and 440 [17,38–40]. The peaks at  $2\theta$  of  $36.28^\circ$ ,  $42.70^\circ$ ,  $55.9^\circ$  and  $62.4^\circ$  represent  $\text{NiAl}_2\text{O}_4$ . It was noted that the peaks of  $\text{ZnAl}_2\text{O}_4$  and  $\text{NiAl}_2\text{O}_4$  were shifted to slightly lower  $2\theta$  values compared to those of stoichiometric  $\text{ZnAl}_2\text{O}_4$  and  $\text{NiAl}_2\text{O}_4$ . This indicated that spinel in obtained nanocomposites was non-stoichiometric. When the reaction temperature was increasing, the diffraction peaks of the samples were slightly expanded (Figure 4). For  $\text{NiAl}_2\text{O}_4$  and  $\text{ZnAl}_2\text{O}_4$  samples, no peak characteristics of  $\text{NiO}$  and  $\text{ZnO}$  were seen, indicating the fine dispersion of these species on the  $\text{NiAl}_2\text{O}_4$  and  $\text{ZnAl}_2\text{O}_4$  supports, respectively, or a possible overlap with the supports' diffraction peaks [41].

### 3.3. SEM Analysis

SEM-EDS results of mixed oxides  $\text{NiO}/\text{ZnO}/\text{Al}_2\text{O}_3$  particles, which were produced at different temperatures (400–800 °C) from initial solutions at 0.2 M concentration, are shown in Figure 5.

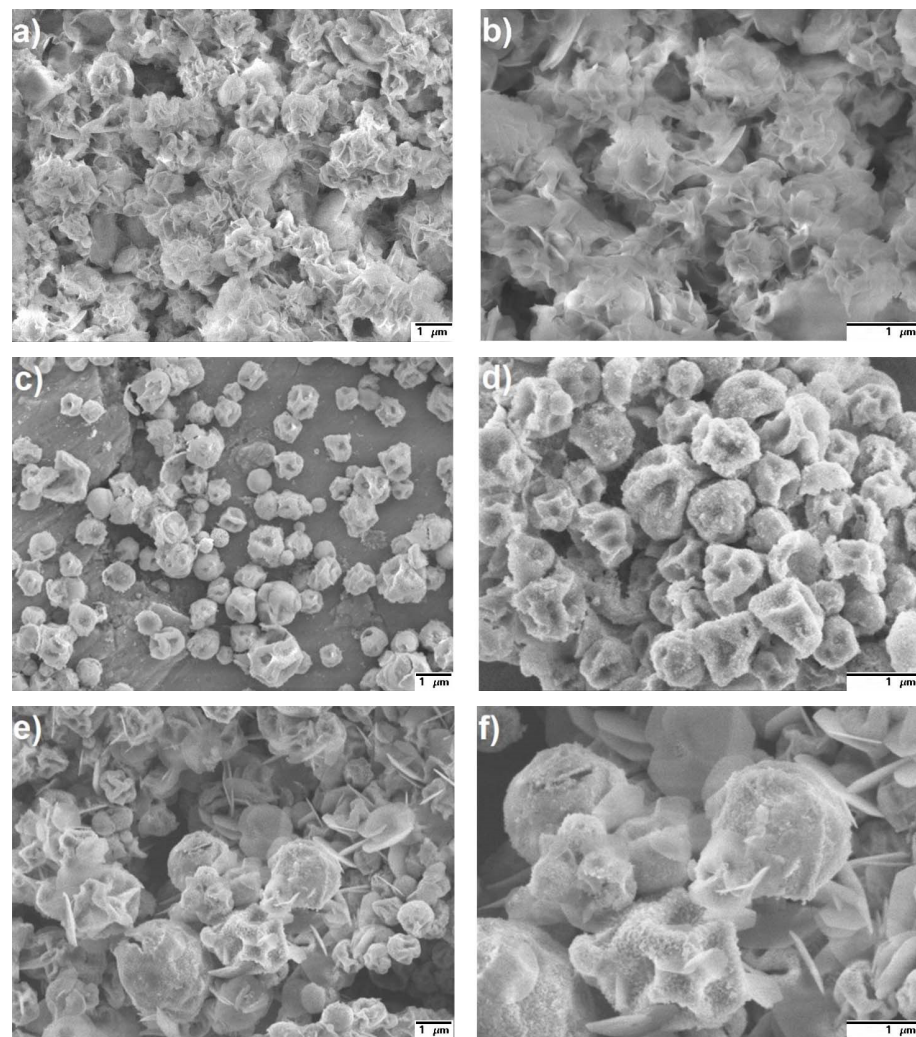


**Figure 5.** SEM results of the NiO/ZnO/Al<sub>2</sub>O<sub>3</sub> particles: (a)  $\times 10,000$ ; (b)  $\times 20,000$  magnification for the samples of 400 °C; (c)  $\times 10,000$ ; (d)  $\times 20,000$  magnification for the samples of 600 °C; (e)  $\times 10,000$ ; (f)  $\times 20,000$  magnification for the samples of 800 °C.

The SEM images show the mixed oxide particles of nearly spherical and some foliated shapes. The size of the particles also varies: primary particles are in the nano range, and submicron size particles are obtained by the aggregation of primary particles. The significant reason for this difference is the temperature effects on aerosol droplets, decomposition reaction and sintering [42,43]. Additionally, particle formation starts with the nucleation of nano-size aerosol droplets, and then secondary particles form by aggregation due to the sintering effect of temperature. A calculation was carried out using the SEM analysis results with the ImageJ program to find the particle size. The results confirmed that the primary particles were nanometer size (Max. = 26.84 nm; Min. = 4.11 nm; Average = 8.65 nm) [44]. When the images were examined, it was determined that the particles have a foliated morphology at 400 °C (Figure 5a,b). Nearly spherical and hollow particles, which began to reshape through intraparticle sintering, replace the foliated morphology at 600 °C (Figure 5c,d). Starting with the appearance of a very irregular shape, both a spherical and foliated morphology were formed at 800 °C (Figure 5e,f). As the temperature increased, the morphology also changed.

EDS analysis was used to investigate the chemical composition of NiO/ZnO/Al<sub>2</sub>O<sub>3</sub> nanoparticles obtained as a result of experimental studies at different temperatures using 0.2 M solution. The existence of nickel, zinc, aluminum and oxygen as elements in EDS

results were determined. In addition, no impurities were detected in the synthesized samples. Table 2 shows the atomic ratios for these analyses.

**Table 2.** EDS results of NiO/ZnO/Al<sub>2</sub>O<sub>3</sub> particles produced at different temperatures.

Molarity (M)/Temperature (°C)	Element (Atomic %)			
	O	Al	Ni	Zn
0.2 M/400 °C	63.5	7.8	18.0	10.7
0.2 M/600 °C	59.2	10.2	18.3	12.3
0.2 M/800 °C	58.7	9.1	17.1	15.1

### 3.4. Raman Analysis

Figure 6 shows the results of Raman analyses of NiO/ZnO/Al<sub>2</sub>O<sub>3</sub> nanoparticles produced at 0.2 M from the initial solutions at different temperatures (400, 600, 800 °C).

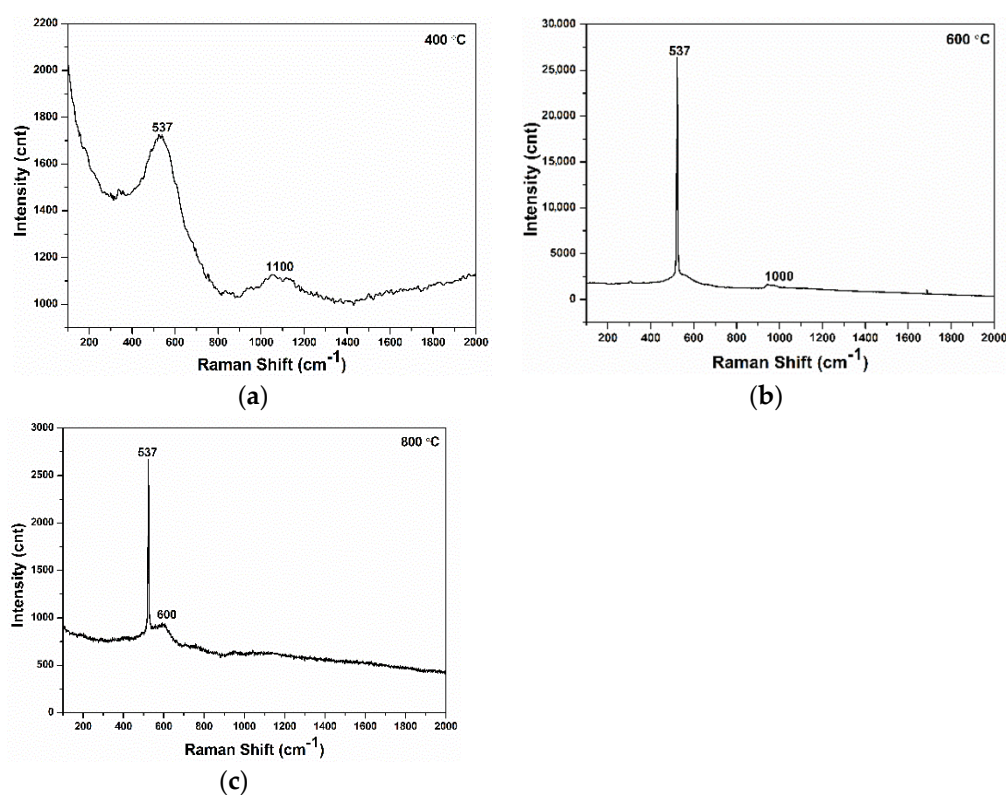


**Figure 6.** Raman spectra of mixed oxides NiO/ZnO/Al<sub>2</sub>O<sub>3</sub> were obtained with different process temperatures: (a) 400 °C; (b) 600 °C; (c) 800 °C.

It is well known that the infrared spectra of spinels are characterized by absorption bands in the range 400–700 cm<sup>-1</sup> [45]. A relatively strong absorption band corresponding to the stretching vibration of the atom in the tetrahedral oxygen environment was located at ~537 cm<sup>-1</sup> and ~600 cm<sup>-1</sup> (Figure 6). NiO has typical emission peaks at ~1000–1100 cm<sup>-1</sup> showing the vibrations occur among Ni–O [39]. Then, the Raman peak of spinels strongly increases at 600 °C and 800 °C, and NiO vibrations decrease and disappear. Increasing the process temperature explains the order of magnitude increase in the Raman signal. The Raman peaks support the observation of the coexistence of NiAl<sub>2</sub>O<sub>4</sub> and ZnAl<sub>2</sub>O<sub>4</sub> phases, as reported in the XRD analysis.

## 4. Conclusions

The present work primarily focuses on the production of mixed oxides NiO/ZnO/Al<sub>2</sub>O<sub>3</sub> nanocomposite particles via the USP method. Secondly, the influence of temperature on both structural and morphology properties of particles was studied. NiO/ZnO/Al<sub>2</sub>O<sub>3</sub>

nanocomposite particles were synthesized in a single step and used a non-cost carrier gas of air in the system. The X-ray diffraction pattern indicated an  $\text{Al}_2\text{O}_3$  phase,  $\text{NiO}-\text{Al}_2\text{O}_3$  systems with spinel phase  $\text{NiAl}_2\text{O}_4$ , and  $\text{ZnO}-\text{Al}_2\text{O}_3$  systems with spinel-phase  $\text{ZnAl}_2\text{O}_4$  [13]. SEM and EDS analyses clearly showed the submicron sized nearly spherical and leafy morphology particles containing Ni, Zn, Al and O elements. It has been determined that the produced  $\text{NiO}/\text{ZnO}/\text{Al}_2\text{O}_3$  nanocomposite particles are composed of primary and secondary particles. The primary particles are nanometer-size (Max. = 26.84 nm; Min. = 4.11 nm; Average = 8.65 nm). On the other hand, with increasing temperature, the sintering and agglomeration mechanism had the most important effect on particle size and morphology. The optimum operating parameters for  $\text{NiO}/\text{ZnO}/\text{Al}_2\text{O}_3$  were determined and the process temperature was 600 °C. According to the results of the Raman analysis at 400 °C, a full conversion did not occur and the presence of NiO was detected. However, no phases other than  $\text{NiAl}_2\text{O}_4$  and  $\text{ZnAl}_2\text{O}_4$  were found at 600 °C and 800 °C. For this reason, since conversion is achieved at a lower temperature of 600 °C, it is more advantageous in terms of cost and provides optimum conditions. This study opens up a promising route for high-quality  $\text{NiO}/\text{ZnO}/\text{Al}_2\text{O}_3$ , as well as various other mixed-oxide nanocomposites.

**Author Contributions:** Conceptualization, D.Y.Ö. and S.G.; methodology, D.Y.Ö. and S.G.; investigation, D.Y.Ö.; writing—original draft preparation, D.Y.Ö., S.G., B.E. and S.S.; supervision, S.G., S.S. and B.F. All authors have read and agreed to the published version of the manuscript.

**Funding:** This research received no external funding.

**Institutional Review Board Statement:** Not applicable.

**Informed Consent Statement:** Not applicable.

**Data Availability Statement:** Data is contained within the article.

**Acknowledgments:** Authors would like to thank; Gültekin Göller, Kürşat Kazmanlı, Fatma Ünal and Hüseyin Sezer for XRD, SEM-EDS and Raman analyses.

**Conflicts of Interest:** The authors declare no conflict of interest.

## References

1. Hussain, F.; Hojjati, M.; Okamoto, M.; Gorga, R.E. Review article: Polymer-matrix Nanocomposites, Processing, Manufacturing, and Application: An Overview. *J. Compos. Mater.* **2006**, *40*, 1511–1575. [[CrossRef](#)]
2. Ravichandran, K.; Praseetha, P.K.; Arun, T.; Gobalakrishnan, S. Chapter 6—Synthesis of Nanocomposites, Synthesis of Inorganic Nanomaterials Advances and Key Technologies. In *Micro and Nano Technologies*; Bhagyaraj, S.M., Oluwafemi, O.S., Kalarikkal, N., Thomas, S., Eds.; Woodhead Publishing: Swaston, UK, 2018; pp. 141–168. [[CrossRef](#)]
3. Juma, A.O.; Matibini, A. Synthesis and structural analysis of ZnO-NiO mixed oxide nanocomposite prepared by homogeneous precipitation. *Ceram. Int.* **2017**, *43*, 15424–15430. [[CrossRef](#)]
4. Juma, A.O.; Arbab, E.A.; Muiva, C.; Lepodise, L.M.; Mola, G.T. Synthesis and characterization of CuO-NiO-ZnO mixed metal oxide nanocomposite. *J. Alloy. Compd.* **2017**, *723*, 866–872. [[CrossRef](#)]
5. Loos, M. Nanoscience and Nanotechnology. In *Carbon Nanotube Reinforced Composites*; CNR Polymer Science and Technology; Elsevier BV: Amsterdam, The Netherlands, 2015; pp. 1–36.
6. El-Nabarawy, T.; Attia, A.; Alaya, M. Effect of thermal treatment on the structural, textural and catalytic properties of the ZnO- $\text{Al}_2\text{O}_3$  system. *Mater. Lett.* **1995**, *24*, 319–325. [[CrossRef](#)]
7. Sajid, S.; Elseman, A.M.; Huang, H.; Ji, J.; Dou, S.; Jiang, H.; Liu, X.; Wei, D.; Cui, P.; Li, M. Breakthroughs in  $\text{NiO}_x$ -HTMs towards stable, low-cost and efficient perovskite solar cells. *Nano Energy* **2018**, *51*, 408–424. [[CrossRef](#)]
8. Goel, R.; Jha, R.; Bhushan, M.; Bhardwaj, R.; Ravikant, C. Hydrothermally synthesized nickel oxide (NiO) nano petals. In *Materials Today: Proceedings*; Elsevier BV: Amsterdam, The Netherlands, 2021.
9. Sharma, R.K.; Kumar, D.; Ghose, R. Synthesis of nanocrystalline ZnO-NiO mixed metal oxide powder by homogeneous precipitation method. *Ceram. Int.* **2016**, *42*, 4090–4098. [[CrossRef](#)]
10. Khudiar, S.S.; Mutlak, F.A.-H.; Nayef, U.M. Synthesis of ZnO nanostructures by hydrothermal method deposited on porous silicon for photo-conversion application. *Optik* **2021**, *247*, 167903. [[CrossRef](#)]
11. Tari, O.; Aronne, A.; Addonizio, M.L.; Daliendo, S.; Fanelli, E.; Pernice, P. Sol-gel synthesis of ZnO transparent and conductive films: A critical approach. *Sol. Energy Mater. Sol. Cells* **2012**, *105*, 179–186. [[CrossRef](#)]
12. Tawale, J.; Dey, K.; Pasricha, R.; Sood, K.; Srivastava, A. Synthesis and characterization of ZnO tetrapods for optical and antibacterial applications. *Thin Solid Films* **2010**, *519*, 1244–1247. [[CrossRef](#)]

13. Mohammed, A.A.; Khodair, Z.T.; Khadom, A.A. Preparation and investigation of the structural properties of  $\alpha$ - $\text{Al}_2\text{O}_3$  nanoparticles using the sol-gel method. *Chem. Data Collect.* **2020**, *29*, 100531. [[CrossRef](#)]
14. Yadav, S.K.; Jeevanandam, P. Synthesis of NiO- $\text{Al}_2\text{O}_3$  nanocomposites by sol-gel process and their use as catalyst for the oxidation of styrene. *J. Alloy. Compd.* **2014**, *610*, 567–574. [[CrossRef](#)]
15. Li, X.; Mu, Z.; Hu, J.; Cui, Z. Gas sensing characteristics of composite NiO/ $\text{Al}_2\text{O}_3$  for 2-chloroethanol at low temperature. *Sens. Actuators B Chem.* **2016**, *232*, 143–149. [[CrossRef](#)]
16. Saedy, S.; Haghighi, M.; Amirkhosrow, M. Hydrothermal synthesis and physicochemical characterization of CuO/ZnO/ $\text{Al}_2\text{O}_3$  nanopowder. Part I: Effect of crystallization time. *Particuology* **2012**, *10*, 729–736. [[CrossRef](#)]
17. Zygmuntowicz, J.; Wicińska, P.; Miazga, A.; Konopka, K. Characterization of composites containing Ni $\text{Al}_2\text{O}_4$  spinel phase from  $\text{Al}_2\text{O}_3$ /NiO and  $\text{Al}_2\text{O}_3$ /Ni systems. *J. Therm. Anal. Calorim.* **2016**, *125*, 1079–1086. [[CrossRef](#)]
18. Macedo, H.P.D.; Medeiros, R.L.B.D.A.; Medeiros, A.L.D.; Oliveira, Â.A.S.D.; Figueredo, G.P.D.; Melo, M.A.D.F.; Melo, D.M.D.A. Characterization of Zn $\text{Al}_2\text{O}_4$  Spinel Obtained by Hydrothermal and Microwave Assisted Combustion Method: A Comparative Study. *Mater. Res.* **2017**, *20*, 29–33. [[CrossRef](#)]
19. Zhang, L.; Yan, J.; Zhou, M.; Yang, Y.; Liu, Y.-N. Fabrication and photocatalytic properties of spheres-in-spheres ZnO/Zn $\text{Al}_2\text{O}_4$  composite hollow microspheres. *Appl. Surf. Sci.* **2013**, *268*, 237–245. [[CrossRef](#)]
20. Crisan, M.; Zaharescu, M.; Kumari, V.D.; Subrahmanyam, M.; Crişan, D.; Drăgan, N.; Răileanu, M.; Jitianu, M.; Rusu, A.; Sadanandam, G.; et al. Sol-gel based alumina powders with catalytic applications. *Appl. Surf. Sci.* **2011**, *258*, 448–455. [[CrossRef](#)]
21. Chen, L.; Zhang, F.; Li, G.; Li, X. Effect of Zn/Al ratio of Ni/ZnO- $\text{Al}_2\text{O}_3$  catalysts on the catalytic deoxygenation of oleic acid into alkane. *Appl. Catal. A Gen.* **2017**, *529*, 175–184. [[CrossRef](#)]
22. Lin, F.; Nordlund, D.; Weng, T.-C.; Moore, R.G.; Gillaspie, D.T.; Dillon, A.C.; Richards, R.M.; Engtrakul, C. Hole Doping in Al-Containing Nickel Oxide Materials to Improve Electrochromic Performance. *ACS Appl. Mater. Interfaces* **2013**, *5*, 301–309. [[CrossRef](#)]
23. Sonawane, G.H.; Patil, S.P.; Sonawane, S.H. Chapter 1-Nanocomposites and Its Applications, Applications of Nanomaterials. In *Micro and Nano Technologies*; Bhagyaraj, S.M., Oluwafemi, O.S., Kalarikkal, N., Thomas, S., Eds.; Woodhead Publishing: Sawston, UK, 2018; pp. 1–22.
24. Messing, G.L.; Zhang, S.-C.; Jayanthi, G.V. Ceramic Powder Synthesis by Spray Pyrolysis. *J. Am. Ceram. Soc.* **1993**, *76*, 2707–2726. [[CrossRef](#)]
25. Hsieh, H.-C.; Yu, J.; Rwei, S.-P.; Lin, K.-F.; Shih, Y.-C.; Wang, L. Ultra-compact titanium oxide prepared by ultrasonic spray pyrolysis method for planar heterojunction perovskite hybrid solar cells. *Thin Solid Films* **2018**, *659*, 41–47. [[CrossRef](#)]
26. Ouhaibi, A.; Ghamnia, M.; Dahamni, M.; Heresanu, V.; Fauquet, C.; Tonneau, D. The effect of strontium doping on structural and morphological properties of ZnO nanofilms synthesized by ultrasonic spray pyrolysis method. *J. Sci. Adv. Mater. Devices* **2018**, *3*, 29–36. [[CrossRef](#)]
27. Lu, Y.; Ma, Y.; Ma, S.; Yan, S. Hierarchical heterostructure of porous NiO nanosheets on flower-like ZnO assembled by hexagonal nanorods for high-performance gas sensor. *Ceram. Int.* **2017**, *43*, 7508–7515. [[CrossRef](#)]
28. Kaur, N.; Zappa, D.; Ferroni, M.; Poli, N.; Campanini, M.; Negrea, R.; Comini, E. Branch-like NiO/ZnO heterostructures for VOC sensing. *Sens. Actuators B Chem.* **2018**, *262*, 477–485. [[CrossRef](#)]
29. Zhu, L.; Zeng, W.; Yang, J.; Li, Y. One-step hydrothermal fabrication of nanosheet-assembled NiO/ZnO microflower and its ethanol sensing property. *Ceram. Int.* **2018**, *44*, 19825–19830. [[CrossRef](#)]
30. Li, J.; Yan, D.; Hou, S.; Lu, T.; Yao, Y.; Chua, D.H.; Pan, L. Metal-organic frameworks derived yolk-shell ZnO/NiO microspheres as high-performance anode materials for lithium-ion batteries. *Chem. Eng. J.* **2018**, *335*, 579–589. [[CrossRef](#)]
31. Kim, K.H.; Yoshihara, Y.; Abe, Y.; Kawamura, M.; Kiba, T. Morphological characterization of sphere-like structured ZnO-NiO nanocomposites with annealing temperatures. *Mater. Lett.* **2016**, *186*, 364–367. [[CrossRef](#)]
32. Mahajan, A.; Deshpande, P.; Butee, S. Synthesis and characterization of NiO/ZnO composite prepared by solid-state reaction method. In *Materials Today: Proceedings*; Elsevier BV: Amsterdam, The Netherlands, 2021. [[CrossRef](#)]
33. Lei, C.; Pi, M.; Xu, D.; Jiang, C.; Cheng, B. Fabrication of hierarchical porous ZnO- $\text{Al}_2\text{O}_3$  microspheres with enhanced adsorption performance. *Appl. Surf. Sci.* **2017**, *426*, 360–368. [[CrossRef](#)]
34. Ullah, R.; Bai, P.; Wu, P.; Etim, U.; Zhang, Z.; Han, D.; Subhan, F.; Ullah, S.; Rood, M.; Yan, Z. Superior performance of freeze-dried Ni/ZnO- $\text{Al}_2\text{O}_3$  adsorbent in the ultra-deep desulfurization of high sulfur model gasoline. *Fuel Process. Technol.* **2017**, *156*, 505–514. [[CrossRef](#)]
35. Li, B.; Yuan, H.; Yang, P.; Yi, B.; Zhang, Y. Fabrication of the composite nanofibers of NiO/ $\gamma$ - $\text{Al}_2\text{O}_3$  for potential application in photocatalysis. *Ceram. Int.* **2016**, *42*, 17405–17409. [[CrossRef](#)]
36. Battiston, S.; Rigo, C.; Severo, E.D.C.; Mazutti, M.A.; Kuhn, R.C.; Gundel, A.; Foletto, E.L. Synthesis of zinc aluminate (Zn $\text{Al}_2\text{O}_4$ ) spinel and its application as photocatalyst. *Mater. Res.* **2014**, *17*, 734–738. [[CrossRef](#)]
37. Du, X.; Li, L.; Zhang, W.; Chen, W.; Cui, Y. Morphology and structure features of Zn $\text{Al}_2\text{O}_4$  spinel nanoparticles prepared by matrix-isolation-assisted calcination. *Mater. Res. Bull.* **2015**, *61*, 64–69. [[CrossRef](#)]
38. Ragupathi, C.; Vijaya, J.J.; Kennedy, L.J. Preparation, characterization and catalytic properties of nickel aluminate nanoparticles: A comparison between conventional and microwave method. *J. Saudi Chem. Soc.* **2017**, *21*, S231–S239. [[CrossRef](#)]

39. Benrabaa, R.; Barama, A.; Boukhlof, H.; Guerrero-Caballero, J.; Rubbens, A.; Bordes-Richard, E.; Löfberg, A.; Vannier, R.-N. Physico-chemical properties and syngas production via dry reforming of methane over NiAl<sub>2</sub>O<sub>4</sub> catalyst. *Int. J. Hydrog. Energy* **2017**, *42*, 12989–12996. [[CrossRef](#)]
40. García-Gómez, N.; Valecillos, J.; Remiro, A.; Valle, B.; Bilbao, J.; Gayubo, A.G. Effect of reaction conditions on the deactivation by coke of a NiAl<sub>2</sub>O<sub>4</sub> spinel derived catalyst in the steam reforming of bio-oil. *Appl. Catal. B Environ.* **2021**, *297*, 120445. [[CrossRef](#)]
41. Rajkumar, T.; Sági, A.; Ábel, M.; Farkas, F.; Gómez-Pérez, J.F.; Kukovecz, Á.; Konya, Z. Ni–Zn–Al-Based Oxide/Spinel Nanostructures for High Performance, Methane-Selective CO<sub>2</sub> Hydrogenation Reactions. *Catal. Lett.* **2019**, *150*, 1527–1536. [[CrossRef](#)]
42. Schneider, C.A.; Rasband, W.S.; Eliceiri, K.W. NIH Image to ImageJ: 25 Years of image analysis. *Nat. Methods* **2012**, *9*, 671–675. [[CrossRef](#)] [[PubMed](#)]
43. Mohaček-Grošev, V.; Vrankić, M.; Maksimović, A.; Mandić, V. Influence of titanium doping on the Raman spectra of nanocrystalline ZnAl<sub>2</sub>O<sub>4</sub>. *J. Alloy. Compd.* **2017**, *697*, 90–95. [[CrossRef](#)]
44. Gurmen, S.; Ebin, B.; Stopić, S.; Friedrich, B. Nanocrystalline spherical iron–nickel (Fe–Ni) alloy particles prepared by ultrasonic spray pyrolysis and hydrogen reduction (USP-HR). *J. Alloy. Compd.* **2009**, *480*, 529–533. [[CrossRef](#)]
45. Ebin, B.; Gençer, Ö.; Gürmen, S. Simple preparation of CuO nanoparticles and submicron spheres via ultrasonic spray pyrolysis (USP). *Int. J. Mater. Res.* **2013**, *104*, 199–206. [[CrossRef](#)]